



OPEN B1 corrected T1 mapping in the differentiation and prediction of breast cancer

Yijie Chen^{1,4}, Jichun Guo^{1,4}, Feifei Shan^{2,4}, Gehua Tong³, Zhihua Meng¹, Zhensong Chen¹ & Junqi Sun¹✉

To explore the effect of B1-corrected T1 mapping on the differentiation of benign and malignant breast lesions and the prediction of biological characteristics in breast carcinoma. 364 patients with breast lesions were included. T1 maps were acquired with multi-flip angle imaging sequences before and after contrast enhancement. T1 values before (T1max, T1mean, T1min) and after enhancement (T1maxce, T1meance, T1mince) were measured. Difference in T1 ($\Delta T1$), percentage reduction in T1 ($\Delta T1\%$) and contrast-enhanced T1 ratio (T1mean/T1meance) were calculated. The differences in T1 values before and after enhancement between benign and malignant breast lesions were compared. Prediction models were constructed with clinical imaging data. The diagnostic efficiency of the prediction models was compared using ROC. DeLong test was used to compare the AUC of the models. Univariate analysis showed that T1mean, T1max, T1meance, T1mince, $\Delta T1$, $\Delta T1\%$, T1mean/T1meance, maximum lesion diameter, age, and BI-RADS classification were statistical significance ($p < 0.05$) between benign and malignant lesions. Multivariate analysis showed that $\Delta T1\%$, age, and BI-RADS classification were independent risk factors. Model 1 ($\Delta T1\%$, age, and BI-RADS classification) demonstrated superior diagnostic performance in differentiating benign from malignant breast lesions, with the AUC of 0.952 (95% CI: 0.926–0.977). B1-corrected T1 mapping has good clinical value for the differentiation of benign and malignant breast lesions.

Keywords B1 corrected T1 mapping, Differentiation, Benign, Malignant, Breast lesions, Biological characteristics, Breast cancer

According to the International Agency for Research on Cancer (IARC), female breast carcinoma is recorded as the second most commonly diagnosed malignancy worldwide in 2020, surpassed only by lung cancer. With respect to mortality, it ranked fourth among all cancer types. Notably, breast cancer represents both the highest incidence and mortality of female cancer worldwide¹. Differentiating between benign and malignant breast lesions poses a significant challenge in clinical imaging diagnosis. The malignant status of breast lesions is the primary basis for determining treatment plans and prognosis^{2,3}. Magnetic Resonance Imaging (MRI) serves as a powerful non-invasive diagnostic tool for evaluating breast lesions. Dynamic Contrast-Enhanced (DCE) MRI detects signals from blood flow within lesions and classifies breast lesions based on time-signal intensity curves according to the BI-RADS system, which provides a grading scale indicating the probability of benign versus malignant lesions. However, due to the long scanning time, overlapping of background parenchymal enhancement and time-intensity curves, DCE MRI has low specificity in the differential diagnosis of benign and malignant breast lesions^{4,5}. A quantitative MRI is needed to improve the accuracy of distinguishing benign and malignant breast lesions.

Multiple laboratory markers assist in distinguishing between benign and malignant breast tumors. The expression status of human epidermal growth factor receptor 2 (HER-2) is critical for molecular subtyping, prognosis evaluation, designing effective treatment strategies, and guiding neoadjuvant chemotherapy, playing a pivotal role in the diagnosis and treatment of breast cancer^{6,7}. Estrogen receptor (ER) and progesterone receptor (PR) are essential for assessing breast cancer prognosis and guiding hormone therapy, particularly for patients with recurrent or metastatic breast cancer^{8,9}. Ki-67, a nuclear antigen indicating tumor cell proliferation, is

¹Department of Radiology, Affiliated Yuebei People's Hospital of Guangdong Medical University, No.133, Huimin South Road, Shaoguan City 512026, Guangdong, China. ²Department of Ultrasound Diagnosis, Affiliated Yuebei People's Hospital of Guangdong Medical University, Shaoguan 512026, Guangdong, China. ³MR Research Collaboration, Siemens Healthineers, Shenzhen 518000, Guangdong, China. ⁴Yijie Chen, Jichun Guo and Feifei Shan contributed equally to this work. ✉email: sunjunqi1233668@126.com

associated with tumor malignancy. Consequently, it serves as a prognostic marker for early breast cancer and aids in guiding chemotherapy for early-stage breast cancer^{10–12}. Breast cancer is highly heterogeneous, leading to varying responses to the same type of tumor treatment among different patients^{13,14}. HER-2, ER, PR, and Ki-67 are associated with the expression of tumor heterogeneity. However, biopsy is an invasive examination that provides only very limited information. Therefore, it is necessary to explore non-invasive quantitative methods to predict the expression of biological characteristics in breast cancer.

T1 mapping enables the derivation of quantitative parameters based on Regions of Interest (ROI), such as T1mean, T1max, and T1min, which reflect tissue-specific pathophysiological changes. Relaxation time is an intrinsic property of tissue, independent of sequence parameters. Previous studies have demonstrated that T1 mapping exhibits excellent repeatability, reproducibility, and accuracy^{15,16}. This technique has shown high diagnostic efficiency in differentiating benign and malignant lesions in the lung, kidney, parotid gland, and liver^{17–21}. Recent studies indicate that T1 values in synthetic MRI can distinguish between benign and malignant breast lesions^{22–26}. However, some research suggests that T1 values may not statistically significantly differentiate between benign and malignant breast lesions^{27,28}. Sensitivity to static field inhomogeneity and partial volume effects can affect the accuracy of T1 values²⁹. Additionally, severe B1 field variations during Variable Flip Angle (VFA) scanning can result in significant T1 value errors between breasts. The B1-corrected T1 mapping technique employs rapid low-angle excitation to acquire T1 maps, significantly reducing scan time while minimizing the impact of B1 field inhomogeneity³⁰. At present, T1 mapping VFA technology is still in the early stage of differentiating benign and malignant breast lesions, it is necessary to explore its potential in distinguishing breast lesions. Therefore, we aimed to explore the effect of B1-corrected T1 mapping on differentiation from benign to malignant breast lesions and the prediction of the expression of biological characteristics (HER-2, Ki-67, PR, ER) in breast cancer.

Subjects and methods

Subjects

This non-randomized, retrospective, and single-center study was performed according to the Declaration of Helsinki (<https://www.wma.net/what-we-do/medical-ethics/declaration-of-helsinki/>), and approved by the Ethics Commission of Yuebei People's Hospital (No. KY-2021-113). Informed consent was obtained from all the participants. From December 2021 to January 2023, 480 patients (482 lesions) with suspected breast lesions underwent T1 mapping MRI examination. Inclusion criteria: (1) female patients; (2) clinically diagnosed breast lesions; (3) no history of breast surgery or chemotherapy before MRI examination; (4) agreement to undergo T1 mapping scans; (5) absence of claustrophobia. Exclusion criteria: (1) the absence of pathological results borderline tumors; (2) lack of imaging data; (3) unclear images; (4) lesions with a diameter smaller than 0.5 cm; (5) borderline tumors. Patients were randomly assigned into two groups in a 2:1 ratio using the random generator function in SPSS 27.0, with two-thirds of the cases in the training group and the remaining cases in the validation group. The flow chart of patient selection was shown in Fig. 1.

MRI acquisition

All examinations were performed using a 3.0 T superconducting MRI system (Siemens MAGNETOM Vida) with an 18-channel phased-array breast surface coil. During the examination, the subject was positioned in a prone position, with both breasts naturally suspended in the recesses of the breast coil. The B1-corrected T1 mapping sequence was added to the conventional clinical MRI protocol. The standard MRI sequences included axial T1-weighted imaging (T1WI), axial T2-weighted imaging (T2WI), fat-suppressed T2-weighted imaging, axial/coronal Dixon dynamic contrast-enhanced imaging, and axial diffusion-weighted imaging (DWI). The parameters for DWI were as follows: repetition time (TR) = 12,100 ms; echo time (TE) = 68 ms; slice thickness = 5 mm; field of view (FOV) = 370 × 370 mm²; b values = 0 and 1000 s/mm²; acquisition time = 105 s.

Routine scanning was performed first, followed by dynamic contrast-enhanced scanning. A high-pressure injector was used to rapidly inject 0.1 mmol/kg of gadopentetate dimeglumine injection (GD-DTPA) (Bayer Medical Care Co., Ltd., Germany) through the elbow vein at a rate of 2 mL/s, followed by a rapid flush with 20 ml of normal saline. Subsequently, dynamic contrast-enhanced MRI was performed using a fast gradient echo sequence with the following parameters: TR = 4.3 ms; TE = 1.6 ms; slice thickness = 1.4 mm; FOV = 360 × 360 mm²; acquisition time = 650 s. VFA axial T1 mapping scans were performed both before and 7 min after contrast injection. The parameters were as follows: TR = 5.2 ms; TE = 2.39 ms; flip angles = 3° and 15°; slice thickness = 4 mm; FOV = 300 mm × 300 mm; image matrix = 135 × 224; number of excitations = 1; receiver bandwidth = 300 kHz; and scan time = 21 s.

Image analysis

All images were uploaded to an image viewer by the researchers. ROIs were first delineated on the axial T1 mapping images, referencing DCE and DWI images. The ROI was manually delineated as a two-dimensional image on the largest slice of the lesion. By referring to DCE MRI and DWI sequences, we avoided cystic and necrotic areas of the lesion and delineated the solid components to reduce the impact of heterogeneity. Additionally, ROIs were delineated by two radiologists to compare inter-observer and intra-observer consistency. The ROIs included the largest possible solid part of the lesion, avoiding partial volume effects, large vessels, cystic necrosis, and hemorrhagic areas. The T1_{mean}, T1_{min}, T1_{max}, T1_{mean} post-contrast enhancement (T1_{meance}), T1 min post-contrast enhancement (T1_{mince}), and T1 max post-contrast enhancement (T1_{maxce}) were automatically calculated for all voxels within each ROI for each subject. The size of the lesion (maximum diameter) was measured and recorded in the image viewer. These measurements were performed by two radiologists with 16 and 2 years of experience in diagnosing breast lesions, who were blinded to the pathological results. One week later, the measurements were repeated by the radiologist with 2 years of experience. The two radiologists discussed discrepancies in

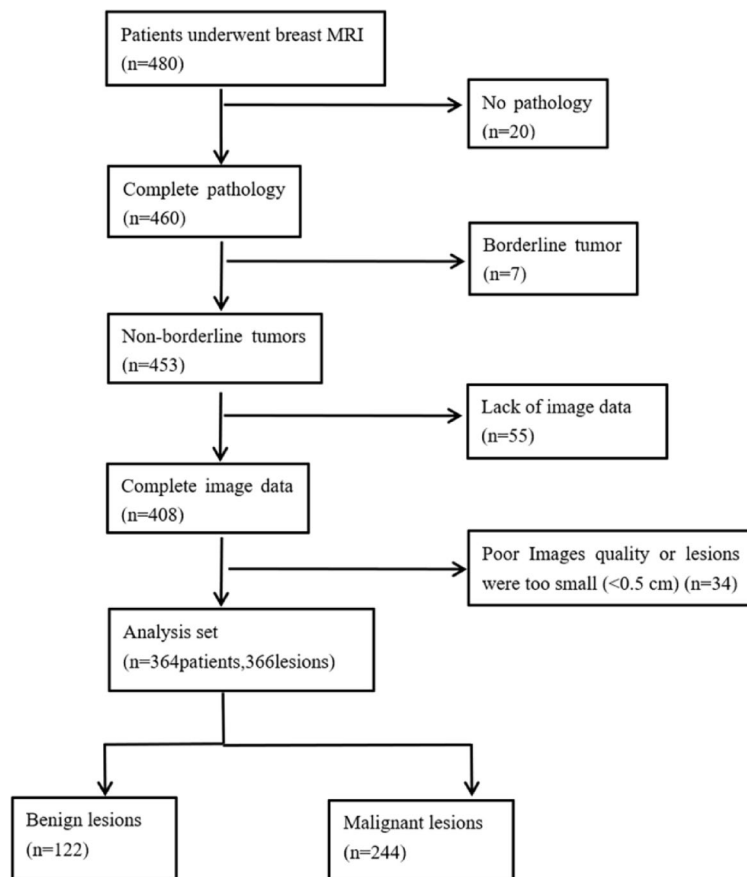


Fig. 1. The flowchart of patient enrollment.

measurements and reached a consensus. Additionally, the BI-RADS scores of breast lesions were extracted from imaging reports. BI-RADS 3 and BI-RADS 4a were classified as benign (likely benign), while BI-RADS 4b, BI-RADS 4c, and BI-RADS 5 were classified as malignant (likely malignant).

Pathologic assessment

The lesion specimens were independently analyzed by two pathologists using hematoxylin and eosin staining and immunohistochemistry results. Any discrepancies in histopathological findings were resolved through discussion. Based on the histopathological diagnosis of the breast lesions from the specimen sections, the lesions were classified into two groups: benign breast lesions and malignant breast lesions. According to the CSCO Breast Cancer Guidelines 2024, the detection criteria for HER-2 were as follows: samples with signals of (+) and (-) were considered negative, while samples with signals of (+++) were considered positive. Samples with (++) signals underwent further in situ hybridization; those showing gene amplification were defined as positive, while those without gene amplification were defined as negative. The Ki-67 expression criteria were as follows: samples were considered positive if $\geq 14\%$ of tumor cells showed positive staining; otherwise, they were considered negative. For ER and PR status, samples were considered positive if $\geq 10\%$ of tumor cells showed positive staining; otherwise, they were considered negative.

The diagnostic efficiency assessment of the prediction models

Receiver operating characteristic (ROC) curve analysis was performed to calculate the area under the curve (AUC), assessing the discriminative ability of the quantitative values for benign versus malignant breast lesions and their predictive capability for breast cancer biological characteristics. The Youden index was used to determine the optimal diagnostic cutoff points, and sensitivity and specificity were calculated. Diagnostic predictive values were expressed by AUC, sensitivity, and specificity. Multivariate analysis was performed on parameters identified as statistically significant in univariate analysis, using logistic regression to construct combinations of statistically significant parameters and establish predictive models. ROC curves were plotted, and the DeLong test was used to compare the diagnostic performance of the models. ROC curves for the models were plotted, and the diagnostic performance of different models was validated.

Statistical analysis

All data analyses were conducted using SPSS version 27.0 software (IBM Corp., Armonk, NY, USA). Quantitative parameters were presented as medians with interquartile ranges in parentheses. Intraclass correlation coefficients

(ICCs) were calculated to assess the inter-rater reliability between the two radiologists (ICC ≥ 0.75 as strong, 0.4–0.75 as moderate, ICC < 0.4 as weak). The Shapiro-Wilk test was used to determine if quantitative data followed a normal distribution. If the data were normally distributed, an independent samples t-test was used to evaluate differences in T1_{mean}, T1_{min}, T1_{max}, T1_{meance}, T1_{mince}, T1_{maxce}, $\Delta T1$, $\Delta T1\%$, and T1_{mean}/T1_{meance} between benign and malignant breast lesions and between breast cancer biological characteristics. If the data were not normally distributed, the Mann-Whitney U test was employed. $p < 0.05$ was considered statistically significant.

Results

Clinical-pathological features

Among the 480 patients with suspected breast lesions who underwent MRI examinations (482 lesions), 116 cases were subsequently excluded. Of these, 20 cases were excluded due to a lack of surgical pathology results, 7 cases were borderline tumors, 55 cases lacked imaging data, and 34 cases had unclear images or small lesion volumes. Ultimately, 366 lesions in 364 patients were analyzed, including a patient with bilateral breast cancer and another patient with breast cancer in one breast and adenosis in the other. Of the 366 breast lesions, 244 were malignant, including 24 of ductal carcinoma in situ, 200 of invasive ductal carcinoma, 3 of mucinous carcinoma, 11 of lobular carcinoma, 2 of metaplastic carcinoma, 1 of malignant phyllodes tumor, and 3 of invasive papillary carcinoma (Table 1). There were 122 benign lesions, including 15 fibroadenomas, 14 inflammatory lesions, 69 adenosis, 4 benign phyllodes tumors, 18 intraductal papillomas, 1 adenomyoepithelioma, and 1 mucinous cystadenomatoid lesion (Table 1). There were 244 patients in the training group and 122 in the validation group. The training group included 156 malignant and 88 benign lesions, while the validation group comprised 88 malignant and 34 benign lesions (Table 1). Figures 2 and 3 showed the representative images of benign and malignant breast lesions.

Consistency testing

The inter-rater ICC values for the quantitative measurements of T1_{mean}, T1_{min}, T1_{max}, T1_{meance}, T1_{mince}, and T1_{maxce} were 0.976, 0.833, 0.955, 0.905, 0.803, and 0.974, respectively, as measured by the two radiologists. One week later, the intra-rater ICC values for the radiologist with 2 years of breast diagnosis experience were 0.970,

Parameters	Values	Percentage (%)
Benign tumors		
Age (years old)	51.29 ± 9.914*	
Max diameter (cm)	2.1 (1.5)**	
Histologic result (no.)		
Fibroadenoma	15	4
Inflammatory lesions	14	3
Adenosis	69	18
Benign phyllodes tumor	4	1
Intraductal papilloma	18	4
Adenomyoepithelioma	1	0.2
mucinous cystic lesion	1	0.2
Malignant tumors		
Age (years old)	46.03 ± 8.804*	
Max diameter (cm)	1.0 (0.8)**	
Histologic result (no.)		
Situ carcinoma	24	6
Invasive ductal carcinoma	200	54
Mucinous carcinoma	3	0.8
Lobular carcinoma	11	3
Metaplastic carcinoma	2	0.5
Malignant Phyllodes tumor	1	0.2
Invasive papillary carcinoma	3	0.8
BIRADS		
2	4	1
3	53	14
4a	50	13
4b	37	10
4c	81	22
5	141	38

Table 1. General characteristics. *, data are mean ± standard deviation. **, median (interquartile distance).

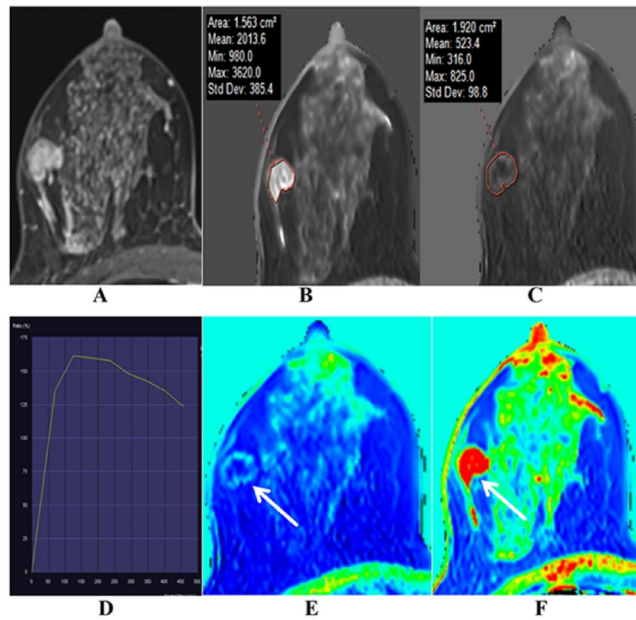


Fig. 2. A 44 years old female was diagnosed as right breast invasive breast cancer by needle biopsy. (A) Enhanced image, a lobulated mass in the right breast with uniform enhancement and clear border; (B) B1 corrected T1 map and its parameters; (C) B1 corrected T1 mapping and parameters after GD contrast agent injection; (D) Dynamic Contrast Enhancement Time Intensity Curve (TIC): outflow type, rapid rise in the early stage and rapid decline later; (E) Pseudocolor plot of B1 corrected T1 map. (F) Pseudocolor plot of B1 corrected T1 map after GD contrast agent injection.

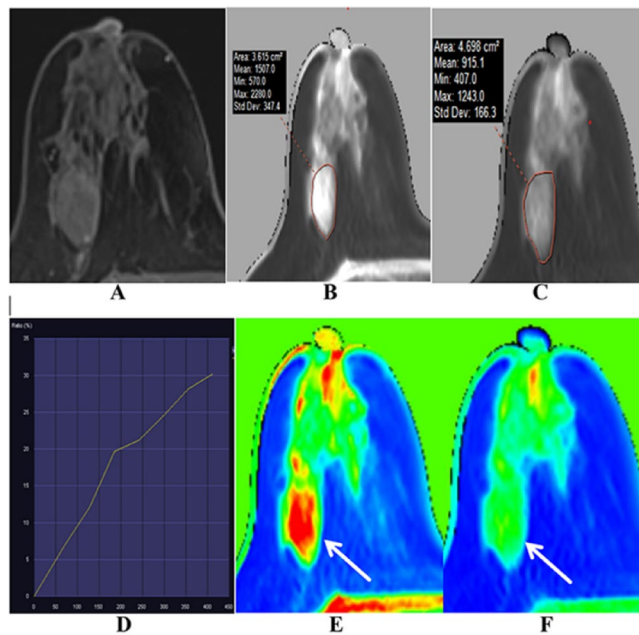


Fig. 3. A 38 years old female was diagnosed as right breast adenosis by needle biopsy. (A) Enhanced image, an elliptical mass in the right breast with uniform enhancement and clear border; (B) B1 corrected T1 map and its parameters; (C) B1 corrected T1 mapping and parameters after GD contrast agent injection; (D) Dynamic Contrast Enhancement Time Intensity Curve (TIC): Inflow type; (E) Pseudocolor plot of B1 corrected T1 map. (F) Pseudocolor plot of B1 corrected T1 map after GD contrast agent injection.

Values	Malignant	Benign	P value	P value (95%CI) (Multivariatel)
T1 _{mean}	1640.7(551.8)	1313.5(554)	<0.001	
T1 _{min}	928.5(347)	897.5(422)	0.650	
T1 _{max}	2245(991.5)	1716(774)	<0.001	
T1 _{meance}	444.5(105.6)	479.5(170)	0.001	
T1 _{mince}	325(81.7)	389(145)	<0.001	<0.001 (1.117–1.411)
T1 _{maxce}	616.5(239.8)	635.5(310)	0.169	
ΔT1	1154.9(501.1)	783(593.8)	<0.001	
ΔT1%	0.72(0.09)	0.61(0.24)	<0.001	0.003 (0.984–0.997)
Max diameter	2.1 (1.5)	1.0 (0.8)	<0.001	0.025(1.033–1.648)
Age*	51.29 ± 9.914	46.03 ± 8.804	<0.001	<0.001 (1.056–1.124)

Table 2. Parametric statistics for identifying benign and malignant lesions. Data are expressed as median (interquartile distance); *, mean ± standard deviation. $\Delta T1 = T1_{mean}/T1_{meance}$; $\Delta T1\% = (T1_{mean}/T1_{meance})/T1_{mean}$.

Value	AUC(95%CI)	Sensitivity	Specificity
T1 _{mean}	0.709(0.652–0.766)	0.721	0.648
T1 _{max}	0.743(0.689–0.796)	0.607	0.779
T1 _{meance}	0.604(0.540–0.668)	0.955	0.238
T1 _{mince}	0.716(0.658–0.775)	0.803	0.549
ΔT1	0.737(0.680–0.795)	0.824	0.582
ΔT1%	0.732(0.673–0.792)	0.873	0.557

Table 3. Diagnostic efficacy of T1 values between malignant and benign lesions. $\Delta T1 = T1_{mean}/T1_{meance}$; $\Delta T1\% = (T1_{mean}/T1_{meance})/T1_{mean}$.

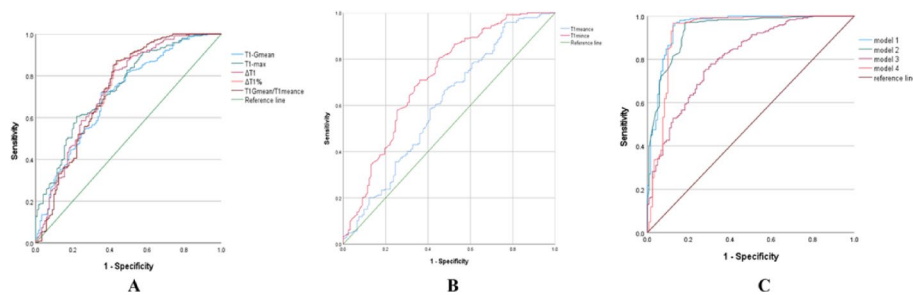


Fig. 4. Receiver operating characteristic (ROC) curve analyses of univariable analyses (A, B) and multivariable analyses (C). $\Delta T1 = T1_{mean} - T1_{meance}$; $\Delta T1\% = (T1_{mean} - T1_{meance})/T1_{mean}$.

0.962, 0.877, 0.938, 0.896, and 0.910, respectively. Excellent inter-rater and intra-rater consistency was observed across the different T1 metrics.

T1 values in differentiating breast lesions

T1_{mean} and ΔT1 passed the normality test, while T1_{mean}, T1_{min}, T1_{max}, T1_{meance}, and T1_{mince} did not. Mann-Whitney U tests showed that T1_{mean}, T1_{max}, ΔT1, ΔT1% and T1_{mean}/T1_{meance} in the malignant breast lesion group were higher than those in the benign lesion group, while the T1_{meance} and T1_{mince} values were lower in the malignant breast lesion group (Table 2). ROC curve analysis revealed that AUC for T1_{max} was the highest (AUC = 0.743), followed by ΔT1 (AUC = 0.737), T1_{mean}/T1_{meance} (AUC = 0.735), ΔT1% (AUC = 0.732), T1_{mince} (AUC = 0.716), and T1_{mean} (AUC = 0.709) (Table 3). The specificities of T1_{mean}, T1_{max}, T1_{meance}, T1_{mince}, ΔT1, ΔT1% and T1_{mean}/T1_{meance} were 0.648, 0.779, 0.238, 0.549, 0.582, 0.557 and 0.566 respectively, with sensitivities of 0.712, 0.607, 0.955, 0.803, 0.824, 0.873 and 0.873 respectively. T1_{max} had the highest specificity, while T1_{meance} had the highest sensitivity (Table 3).

Application of models in differentiating breast lesions

Univariate analysis showed that T1_{mean}, T1_{max}, T1_{meance}, T1_{mince}, ΔT1, ΔT1%, T1_{mean}/T1_{meance}, maximum diameter, age, and BI-RADS classification were statistical different in differentiating from benign to malignant breast lesions ($p < 0.05$, Fig. 4). Multivariate analysis showed that ΔT1%, age, and BI-RADS classification were

Values	AUC(95%CI)	Sensitivity	Specificity
Model 1	0.954(0.927–0.980)	0.975	0.861
Model 2	0.750(0.692–0.808)	0.824	0.590
Model 3	0.932(0.897–0.967)	0.967	0.861
Model 4	0.893(0.851–0.936)	0.967	0.820

Table 4. Diagnostic efficacy of predict models between malignant and benign lesions. Model 1 = age + maximum diameter + BIRADS + T1mince + $\Delta T1\%$; Model 2 = T1mince + $\Delta T1\%$; Model 3 = BI-RADS + T1mince + $\Delta T1\%$; Model4 = BIRADS.

Variables	Training validation				Validation groups			
	Model 1	Model 2	Model 3	Model 4	Model 1	Model 2	Model 3	Model 4
AUC (95%CI)	0.936 (0.898–0.975)	0.730 (0.657–0.803)	0.909 (0.860–0.958)	0.869 (0.812–0.926)	0.993 (0.983–1.000)	0.799 (0.708–0.890)	0.984 (0.962–1.000)	0.939 (0.882–0.996)
Sensitivity	0.963	0.834	0.951	0.963	0.963	0.840	0.975	0.975
Specificity	0.825	0.587	0.825	0.775	0.976	0.683	0.951	0.902
Accuracy	0.910	0.770	0.910	0.900	0.975	0.795	0.967	0.951
F1 score	0.910	0.740	0.910	0.900	0.975	0.775	0.967	0.951

Table 5. Diagnostic efficacy of B1 corrected T1 mapping in both the training and validation groups.

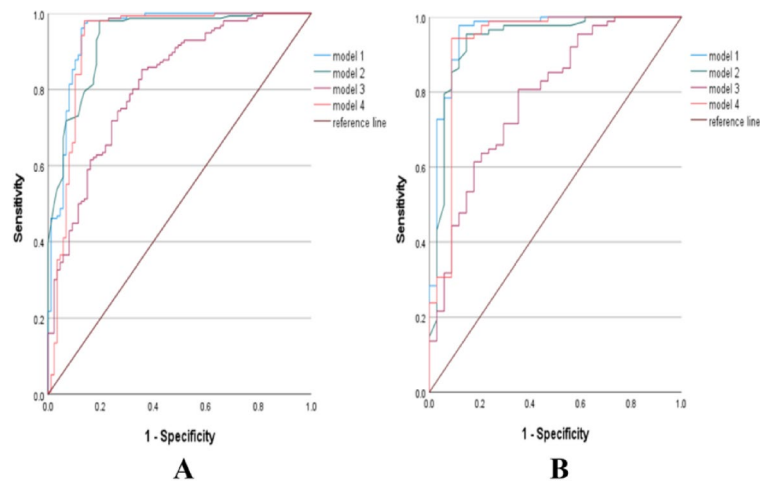


Fig. 5. Receiver operating characteristic (ROC) curve analyses of the training validation groups (A) and validation groups (B).

independent risk factors. Four prediction models were established based on these parameters, namely Model 1 (BIRADS classification, age, and $\Delta T1\%$), Model 2 (BI-RADS classification and age), Model 3 (age and $\Delta T1\%$), and Model 4 (BI-RADS classification and $\Delta T1\%$). ROC analysis showed that the AUC values for Models 1, 2, 3, and 4 were 0.952, 0.936, 0.809, and 0.925 respectively (Table 4). Models 1, 2, and 4 had significantly higher AUC values than Model 3 ($Z = 6.72, p < 0.001$; $Z = 4.98, p < 0.001$; $Z = -4.76, p < 0.001$), and Model 1 had a significantly higher AUC value than Model 4 ($Z = 3.03, p = 0.002$). There were no statistically significant disparities in AUC values between Models 1 and 2, as well as Models 2 and 4. In the training and validation groups, Model 1 showed the best diagnostic efficacy in differentiating between benign and malignant breast lesions, with AUC of 0.950 and 0.957, sensitivity of 0.974, 0.864, and specificity of 0.977 and 0.882, respectively. Model 4 had the highest specificity in discriminating from benign to malignant breast lesions, with the specificities of 0.864 and 0.912, respectively (Table 5; Fig. 5).

T1 values in biological features of breast cancer

$T1_{mean}$, $T1_{max}$, $T1_{min}$, $T1_{meance}$, $T1_{maxce}$, and $\Delta T1$ can differentiate HER-2 positive and negative groups in breast cancer, with the HER-2 positive group exhibiting higher T1 values than the HER-2 negative group. Significant disparities were found between Ki-67 positive and negative groups regarding $T1_{mean}$, $T1_{max}$, $T1_{min}$, $T1_{meance}$, $T1_{maxce}$, and

Items	Her-2		Ki-67		PR		ER	
	P	AUC (95%CI)	P	AUC (95%CI)	P	AUC (95%CI)	P	AUC (95%CI)
T1 _{mean}	0.004	0.614 (0.542–0.687)	0.008	0.619 (0.533–0.706)	0.066		0.250	
T1 _{min}	0.220		0.015	0.609 (0.526–0.693)	0.273		0.656	
T1 _{max}	0.046	0.578 (0.504–0.653)	0.034	0.595 (0.504–0.685)	0.443		0.799	
T1 _{meance}	0.005	0.611 (0.536–0.685)	0.001	0.654 (0.573–0.735)	0.070		0.095	
T1 _{mince}	0.561		0.950		0.997		0.808	
T1 _{maxce}	< 0.001	0.673 (0.599–0.747)	< 0.001	0.695 (0.620–0.769)	0.012	0.601 (0.524–0.678)	0.005	0.623 (0.536–0.710)
ΔT1	0.024	0.588 (0.514–0.662)	0.034	0.595 (0.508–0.683)	0.121		0.347	
ΔT1%	0.610		0.896		0.787		0.982	

Table 6. B1 corrected T1 mapping about the expression of HER-2, Ki-67, PR and ER. $\Delta T1 = T1_{mean} - T1_{meance}$; $\Delta T1\% = (T1_{mean} - T1_{meance}) / T1_{mean}$.

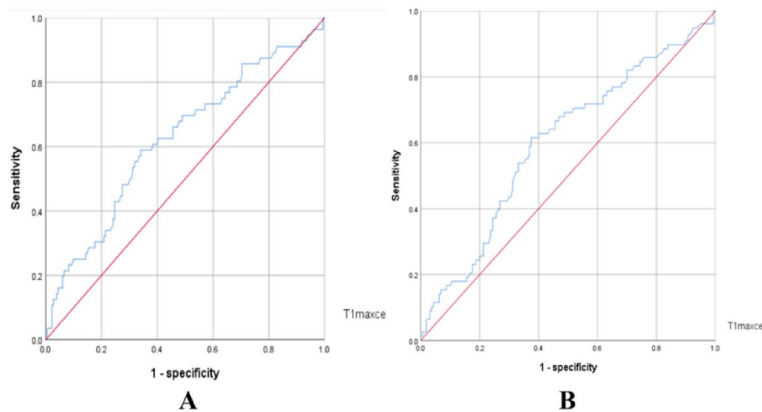


Fig. 6. Receiver operating characteristic (ROC) curves of the Her-2(A), Ki-67(B), PR(C) and ER(D). $\Delta T1 = T1_{mean} - T1_{meance}$; $\Delta T1\% = (T1_{mean} - T1_{meance}) / T1_{mean}$.

ΔT1 values, with the Ki-67 positive group showing higher values than the negative group. T1_{maxce} can differentiate PR positive and negative groups, as well as ER positive and negative groups. Specifically, the T1_{maxce} were lower in the ER positive and PR positive groups compared to the ER negative and PR negative groups. In HER-2 positive and negative groups, $AUC(T1_{maxce}) > AUC(T1_{mean}) > AUC(T1_{meance}) > AUC(\Delta T1) > AUC(T1_{max})$. In Ki-67 positive and negative groups: $AUC(T1_{maxce}) > AUC(T1_{meance}) > AUC(T1_{mean}) > AUC(T1_{min}) > AUC(T1_{max}) = AUC(\Delta T1)$. The AUC values for T1_{maxce} in the ER positive and negative groups, as well as PR positive and negative groups, were 0.623 and 0.601 (Table 6; Fig. 6).

Discussion

The differentiation of benign and malignant breast lesions has always been a clinically significant issue. Determining the biological characteristics of breast cancer facilitates precision treatment based on the lesion's molecular subtype. In this study, we utilized B1-corrected T1 mapping to quantitatively evaluate breast lesions, transforming the subjective assessment of different tissues by conventional MRI into quantitative and objective evaluation. We found that T1_{mean}, T1_{max}, T1_{mince}, ΔT1, ΔT1% and T1_{mean}/T1_{meance} demonstrated excellent diagnostic efficacy between benign and malignant breast lesions, with further improvement in diagnostic performance when combined with age and BI-RADS classification. Regarding the biological characteristics of breast cancer, T1_{mean}, T1_{max}, T1_{meance}, T1_{maxce}, and ΔT1 could predict HER-2 expression. T1_{mean}, T1_{min}, T1_{max}, T1_{meance}, T1_{maxce}, and ΔT1 could predict Ki-67 expression. T1_{maxce} could predict PR and ER expressions. B1-corrected T1 mapping may be used to supplement preoperative biopsy.

Currently, commonly used T1 mapping techniques in breast imaging include Look Locker and VFA^{22,30}. The Look Locker technique, based on inversion recovery, is insensitive to static field inhomogeneities (with a measurement deviation of less than 5% for T1), but it has low spatial resolution and long acquisition times. VFA, on the other hand, acquires T1 images using at least two different flip angles and enables single-breath-hold acquisition with higher spatial resolution. However, VFA is highly sensitive to motion due to the small flip angles used and is susceptible to B1 field inhomogeneities. In this study, the small-angle flip technique and B1 field correction were utilized to mitigate the effects of B1 inhomogeneities, which significantly improved image quality and the accuracy of quantitative measurements. Additionally, acquisition times were greatly reduced, enhancing the feasibility and reproducibility of the study.

The T1 value is an intrinsic property of substances that reflects physiological changes within lesions and is related to parameters such as macromolecule concentration and water content in tissues^{31,32}. In this study, $T1_{\text{mean}}$, $T1_{\text{max}}$, $T1_{\text{meance}}$, $T1_{\text{mince}}$, $\Delta T1$, $\Delta T1\%$, and the $T1_{\text{mean}}/T1_{\text{meance}}$ ratio were found to be statistically significant in distinguishing between benign and malignant breast lesions. This finding is consistent with previous studies, in which pre-contrast $T1_{\text{mean}}$ can effectively differentiate between benign and malignant breast lesions^{22–24}. Among the pre-contrast quantitative T1 values, malignant lesions exhibited higher T1 values compared to benign lesions, likely because the T1 relaxation time reflects the energy transfer between the nuclei of the spin group and the surrounding external environment. In malignant breast tumors, the extracellular matrix associated with cellular necrosis is more abundant, particularly in rapidly growing and highly malignant tumors, leading to longer T1 relaxation times.

Additionally, deoxyhemoglobin levels are higher in malignant tumors compared to benign lesions^{33,34}. Oxygen, having a paramagnetic effect, shortens the T1 relaxation time. Therefore, the T1 relaxation time is longer in malignant lesions than in benign ones. Li et al. demonstrated that the post-contrast T1 standard deviation is statistically significant²⁵. Although we did not analyze the T1 standard deviation, we found that $T1_{\text{mean}}$ values in malignant lesions were significantly lower than those in benign lesions. This is likely because post-contrast T1 values reflect the concentration of contrast agent in the extracellular space^{35,36}. The high blood flow and rapid passage of contrast agent in malignant lesions, due to extensive neovascularization, result in shorter retention times and lower extracellular concentrations. In this study, we observed that $\Delta T1$ and $\Delta T1\%$ were greater in malignant tumors compared to benign tumors, which is consistent with the findings of Matsuda et al.²² and He et al.²⁶. $\Delta T1$ and $\Delta T1\%$ represent changes in contrast agent concentration within the tumor, indirectly reflecting the different hemodynamic characteristics of the lesions. In malignant tumors, faster tumor growth requires more nutrients, leading to increased angiogenesis and faster contrast agent passage through the tumor, resulting in higher $\Delta T1$ and $\Delta T1\%$. Although $\Delta T1$ and $\Delta T1\%$ may indicate the malignancy of the tumor, further validation is needed. On the other hand, other studies have suggested that quantitative T1 values cannot distinguish between benign and malignant breast lesions^{27,28}, which contradicts our findings. This discrepancy may be attributed to differences in the total sample size and the proportion of pathological subtypes of benign and malignant lesions. This may be associated with factors such as the proportions of pathological subtypes of benign and malignant lesions, ROI contouring methods, and inclusion/exclusion criteria, which can be analyzed by establishing subgroups and comparing different ROI contouring methods.

Model 1 (BIRADS classification, age, and $\Delta T1\%$) demonstrated the optimal diagnostic performance. BIRADS classification assesses the benign and malignant breast lesions by morphology, margins, growth patterns, and enhancement patterns; it is associated with the diagnosing physician's experience and thus exhibits high subjectivity when used alone. $\Delta T1\%$ is a quantitative parameter that accurately reflects hemodynamic changes in benign and malignant lesions, but it is susceptible to the influence of lesion heterogeneity. The age range of patients included in this study was concentrated between 43 and 56 years, which corresponds to the peak age of breast cancer incidence in Asian women, and breast cancer incidence is positively correlated with age. The AUC value of the combined model of these three parameters was higher than that of single-parameter models, thereby improving the accuracy of differential diagnosis between benign and malignant lesions.

In this study, all cases were randomly divided into a training group and a validation group in a 2:1 ratio. Statistical analysis of T1 values in the training and validation groups was conducted, resulting in a predictive model that demonstrated good stability in distinguishing between benign and malignant breast lesions. To enhance the reliability and reproducibility of the study, inter-rater and intra-rater ICC were performed, showing excellent consistency among various quantitative values. The ICC values for $T1_{\text{min}}$, $T1_{\text{max}}$, $T1_{\text{mince}}$, and $T1_{\text{maxce}}$ were lower than those for $T1_{\text{mean}}$ and $T1_{\text{meance}}$. This discrepancy may be attributed to manual errors by different clinicians when delineating the ROIs for $T1_{\text{max}}$ and $T1_{\text{min}}$, as $T1_{\text{max}}$ and $T1_{\text{min}}$ are individual pixel values.

In our study, $T1_{\text{mean}}$, $T1_{\text{min}}$, $T1_{\text{max}}$, $T1_{\text{meance}}$, $T1_{\text{maxce}}$, and $\Delta T1$ are statistically significant in predicting Ki-67 expression. The pre-contrast $T1_{\text{mean}}$, $T1_{\text{min}}$, and $T1_{\text{max}}$ in the Ki-67(+) group were higher than those in the Ki-67(-) group, which is consistent with the findings reported by Matsuda M et al.^{37,38}. Ki-67 plays a central role in structuring chromosomes throughout the mitotic cell cycle and is closely associated with the degree of cellular proliferation^{39–41}. Ki-67(+) suggests accelerated protein synthesis and increased macromolecular density, resulting in prolonged T1 relaxation times. The higher $T1_{\text{meance}}$ and $T1_{\text{maxce}}$ in the Ki-67(+) group compared to the Ki-67(-) group. This may be due to the enhanced angiogenesis ability of epithelial cells in Ki-67(+) lesion⁴², which accelerates contrast agent extravasation and washout kinetics. The structural heterogeneity of malignant lesions may also contribute to this effect, as necrotic regions within the inner capsule reduce the local concentration of contrast agent through dilution. The higher $\Delta T1$ values in the Ki-67(+) group compared to the Ki-67(-) group. Ki-67(+) may indicate higher-grade malignancies. Ki-67(+) may correlate with higher grade malignancies due to their elevated vascular density and permeability, which enhance peak contrast enhancement. $T1_{\text{mean}}$, $T1_{\text{max}}$, $T1_{\text{meance}}$, $T1_{\text{maxce}}$, and $\Delta T1$ were statistically significant in predicting Her-2 expression in our study. The pre-contrast $T1_{\text{mean}}$, $T1_{\text{max}}$ in the Her-2(+) group were higher than those in the Her-2(-) group. HER-2 primarily regulates cell proliferation, differentiation, and apoptosis through the PI3K/AKT signaling pathway while also stimulating tumor angiogenesis^{43,44}. Her-2(+) status enhances cellular proliferation and differentiation within the lesion, which exhibits the highest degree of mucin necrosis and consequently elevated T1 values. The pre-contrast $T1_{\text{mean}}$, $T1_{\text{max}}$ and $\Delta T1$ in Her-2(+) group were higher than those in Her-2(-) group. It may be related to the growth of neovascularization in the lesion and the retention time of contrast agent in the lesion. $T1_{\text{maxce}}$ was statistically significant in predicting ER and PR expression in our study. Compared with ER (-) group, $T1_{\text{maxce}}$ was lower in ER (+) group, which was consistent with the result of PR group. Estrogen receptors suppress vascular endothelial growth factor overexpression, slowing neovascularization in the lesion⁴⁵. It decreases contrast agent extravasation into the tumor microenvironment,

ultimately lowering T1 value. Progesterone receptor expression depends on estrogen. Progesterone receptor can inhibit cell proliferation⁴⁶, which decreases T1 value.

This study also has several limitations. Firstly, it is a single-center study. T1 values were acquired using a single MRI scanner, specific scanning parameters may cause T1 values to be dependent on the device. Additionally, the study population drawn from the same region with regional bias, due to regional lifestyle and environmental factors, which could constrain the study generalizability. They may influence the diagnostic accuracy and predictive capacity of T1 values. The reproducibility of our results needs to be further tested by multicenter studies. Thirdly, there may be heterogeneity in observed lesion size on the same slice among different MRI contrasts, and manual delineation of ROIs may incur deviations. In this study, inter-group measurements were repeated by two radiologists and consistency was assessed. Moreover, we delineated 2D ROIs on the slice where the lesion appeared largest. The 3D ROI would better reflect the overall condition inside the entire lesion. We plan to address this issue in future studies. Finally, device dependence is a limitation of this study. Next, we plan to improve the stability of the model by collecting cases from multiple hospitals in different regions and compare the impact of different devices on the discriminative efficacy of quantitative parameters.

Conclusion

In conclusion, the B1-corrected T1 mapping technique has great potential in differentiating benign and malignant breast lesions and predicting tumor markers in breast cancer. $T1_{\text{mean}}$, $T1_{\text{max}}$, $T1_{\text{meance}}$, and $T1_{\text{mince}}$ can serve as markers for the preliminary diagnosis of breast lesions, and the models can enhance diagnostic efficacy. $T1_{\text{maxce}}$ can predict the expression of biological characteristics of breast cancer, optimizing clinical treatment strategies for breast cancer. Further validation is needed through multicenter studies with larger sample sizes.

Data availability

The datasets used and/or analysed during the current study available from the corresponding author on reasonable request.

Received: 4 March 2025; Accepted: 8 August 2025

Published online: 21 August 2025

References

- Bray, F. et al. Jemal a.global cancer statistics 2022: GLOBOCAN estimates of incidence and mortality worldwide for 36 cancers in 185 countries. *CA Cancer J. Clin.* **74** (3), 229–263 (2024).
- Kunkler, I. H. et al. Breast-Conserving surgery with or without irradiation in early breast Cancer. *N Engl. J. Med.* **388** (7), 585–594 (2023).
- Laws, A. & Punglia, R. S. Endocrine therapy for primary and secondary prevention after diagnosis of High-Risk breast lesions or preinvasive breast Cancer. *J. Clin. Oncol.* **41** (17), 3092–3099 (2023).
- Pinker, K. et al. The potential of multiparametric MRI of the breast. *Br. J. Radiol.* **90** (1069), 20160715 (2017).
- Panigrahi, B. et al. An abbreviated protocol for High-risk screening breast magnetic resonance imaging: impact on performance metrics and BI-RADS Assessment. *Acad. Radiol.* **24** (9), 1132–1138 (2017).
- Hurvitz, S. A. et al. Trastuzumab Deruxtecan versus trastuzumab emtansine in patients with HER2-positive metastatic breast cancer: updated results from DESTINY-Breast03, a randomised, open-label, phase 3 trial. *Lancet* **401** (10371), 105–117 (2023).
- Lin, N. U. et al. Tucatinib vs placebo, both in combination with trastuzumab and capecitabine, for previously treated ERBB2 (HER2)-Positive metastatic breast cancer in patients with brain metastases: updated exploratory analysis of the HER2CLIMB randomized clinical Trial. *JAMA Oncol.* **9** (2), 197–205 (2023).
- Chapman, J. W. et al. Adjunctive statistical standardization of adjuvant Estrogen receptor and progesterone receptor in Canadian cancer trials group MA.27 postmenopausal breast cancer trial of exemestane versus Anastrozole. *J. Clin. Oncol.* **42** (24), 2887–2898 (2024).
- Xiao, Y. et al. Progesterone receptor impairs immune respond and down-regulates sensitivity to anti-LAG3 in breast cancer. *Transl Res.* **271**, 68–78 (2024).
- Whelan, T. J. et al. Omitting radiotherapy after breast-Conserving surgery in luminal A breast Cancer. *N Engl. J. Med.* **389** (7), 612–619 (2023).
- Will, M. et al. Therapeutic resistance to anti-oestrogen therapy in breast cancer. *Nat. Rev. Cancer.* **23** (10), 673–685 (2023).
- Lee, J. et al. Ki-67, 21-Gen recurrence score, endocrine resistance, and survival in patients with breast Cancer. *JAMA Netw. Open.* **6** (8), e2330961 (2023).
- Loi, S. et al. Effects of Estrogen receptor and human epidermal growth factor receptor-2 levels on the efficacy of trastuzumab: A secondary analysis of the HERA Trial. *JAMA Oncol.* **2** (8), 1040–1047 (2016).
- Seol, H. et al. Intratumoral heterogeneity of HER2 gene amplification in breast cancer: its clinicopathological significance. *Mod. Pathol.* **25** (7), 938–948 (2012).
- Jiang, J. et al. B₁-Corrected T1 mapping in lung cancer: repeatability, reproducibility, and identification of histological Types. *J. Magn. Reson. Imaging.* **54** (5), 1529–1540 (2021).
- Sorace, A. G. et al. Repeatability, reproducibility, and accuracy of quantitative mri of the breast in the community radiology setting. *J. Magn. Reson. Imaging.* **23** <https://doi.org/10.1002/jmri.26011> (2018).
- Yang, S. et al. A pilot study of native T1-mapping for focal pulmonary lesions in 3.0 T magnetic resonance imaging: size Estimation and differential diagnosis. *J. Thorac. Dis.* **12** (5), 2517–2528 (2020).
- Wang, S. et al. Contrast-enhanced magnetic resonance (MR) T1 mapping with low-dose gadolinium-diethylenetriamine pentaacetic acid (Gd-DTPA) is promising in identifying clear cell renal cell carcinoma histopathological grade and differentiating fat-poor angiomyolipoma. *Quant. Imaging Med. Surg.* **10** (5), 988–998 (2020).
- Yan, Q. et al. Preliminary study of 3 T-MRI native T1-mapping radiomics in differential diagnosis of non-calcified solid pulmonary nodules/masses. *Cancer Cell. Int.* **21** (1), 539 (2021).
- Wang, F. et al. 3D variable flip angle T1 mapping for differentiating benign and malignant liver lesions at 3T: comparison with diffusion weighted imaging. *BMC Med. Imaging.* **22** (1), 146 (2022).
- Wen, B. et al. Value of pre-/post-contrast-enhanced T1 mapping and readout segmentation of long variable echo-train diffusion-weighted imaging in differentiating Parotid gland tumors. *Eur. J. Radiol.* **162**, 110748 (2023).
- Lian, C. et al. The diagnostic performance of T1 mapping in the assessment of breast lesions: A preliminary study. *Eur. J. Radiol.* **177**, 111589 (2024).

23. Matsuda, M. et al. Enhanced masses on Contrast-Enhanced breast: differentiation using a combination of dynamic Contrast-Enhanced MRI and quantitative evaluation with synthetic MRI. *J. Magn. Reson. Imaging*. **53** (2), 381–391 (2021).
24. Meng, L. et al. Evaluation of the differentiation of benign and malignant breast lesions using synthetic relaxometry and the Kaiser score. *Front. Oncol.* **12**, 964078 (2022).
25. Li, X. et al. Synthetic MRI in breast cancer: differentiating benign from malignant lesions and predicting immunohistochemical expression status. *Sci. Rep.* **13** (1), 17978 (2023).
26. He, H. et al. Multiparametric MRI model with synthetic MRI, DWI multi-quantitative parameters, and differential sub-sampling with cartesian ordering enables BI-RADS 4 lesions diagnosis with high accuracy. *Front. Oncol.* **13**, 1180131 (2024).
27. Liu, J. et al. Synthetic MRI, multiplexed sensitivity encoding, and BI-RADS for benign and malignant breast cancer discrimination. *Front. Oncol.* **12**, 1080580 (2023).
28. Gao, W. et al. Quantitative assessment of breast tumor: comparison of four methods of positioning region of interest for synthetic relaxometry and diffusion Measurement. *Acad. Radiol.* ; **19**: (2024). S1076-6332(24)00135-1.
29. Bedair, R. et al. Effect of radiofrequency transmit field correction on quantitative dynamic Contrast-enhanced MR imaging of the breast at 3.0 T. *Radiology* **279** (2), 368–377 (2016).
30. Serry, F. M. et al. Dual flip-angle IR-FLASH with spin history mapping for B1 + corrected T1 mapping: application to T1 cardiovascular magnetic resonance multitasking. *Magn. Reson. Med.* **86** (6), 3182–3191 (2021).
31. Taylor, A. J. et al. T1 mapping: basic techniques and clinical applications. *JACC Cardiovasc. Imaging*. **9** (1), 67–81 (2016).
32. Ioannou, A. et al. Tracking treatment response in cardiac Light-Chain amyloidosis with native T1 Mapping. *JAMA Cardiol.* **8** (9), 848–852 (2023).
33. Zhu, Q. et al. Assessment of functional differences in malignant and benign breast lesions and improvement of diagnostic accuracy by using US-guided diffuse optical tomography in conjunction with conventional US. *Radiology* **280** (2), 387–397 (2016).
34. Calamante, F. et al. Early changes in water diffusion, perfusion, T1, and T2 during focal cerebral ischemia in the rat studied at 8.5 T. *Magn. Reson. Med.* **41** (3), 479–485 (1999).
35. Tirkes, T. et al. Quantitative MR evaluation of chronic pancreatitis: extracellular volume fraction and MR relaxometry. *AJR Am. J. Roentgenol.* **210**, 533–542 (2018).
36. Adams, L. C. et al. Assessment of the extracellular volume fraction for the grading of clear cell renal cell carcinoma: first results and histopathological findings. *Eur. Radiol.* **29**, 5832–5843 (2019).
37. Matsuda, M. et al. Utility of synthetic MRI in predicting the Ki-67 status of oestrogen receptor-positive breast cancer: a feasibility study. *Clin Radiol.* ;75(5): 398.e1-398.e8. (2020).
38. Li, G. et al. Native T1-mapping and diffusion-weighted imaging (DWI) can be used to identify lung cancer pathological types and their correlation with Ki-67 expression. *J. Thorac. Dis.* **14** (2), 443–454 (2022).
39. van Schaik, T. et al. Dynamic chromosomal interactions and control of heterochromatin positioning by Ki-67. *EMBO Rep.* **23** (12), e55782 (2022).
40. Booth, D. G. et al. 3D-CLEM reveals that a major portion of mitotic chromosomes is not Chromatin. *Mol. Cell.* **64** (4), 790–802 (2016).
41. Mrouj, K. et al. Ki-67 regulates global gene expression and promotes sequential stages of carcinogenesis. *Proc. Natl. Acad. Sci. U S A.* **118** (10), e2026507118 (2021).
42. Li, Z. et al. Apoptotic vesicles activate autophagy in recipient cells to induce angiogenesis and dental pulp regeneration. *Mol. Ther.* **30** (10), 3193–3208 (2022).
43. Kallergi, G. et al. Phosphorylated EGFR and PI3K/Akt signaling kinases are expressed in Circulating tumor cells of breast cancer patients. *Breast Cancer Res.* **10** (5), R80 (2008).
44. Hosonaga, M. et al. Expression of CD24 is associated with HER2 expression and supports HER2-Akt signaling in HER2-positive breast cancer cells. *Cancer Sci.* **105** (7), 779–787 (2014).
45. Ludovini, V. et al. Evaluation of the prognostic role of vascular endothelial growth factor and microvessel density in stages I and II breast cancer patients. *Breast Cancer Res. Treat.* **81** (2), 159–168 (2003).
46. Mohammed, H. et al. Progesterone receptor modulates ER α action in breast cancer. *Nature* **523** (7560), 313–317 (2015).

Acknowledgements

We are thankful to participants and funding parties to support this study.

Author contributions

Guarantor of integrity of the entire study: Junqi Sun Study concepts: Junqi Sun Study design: Junqi Sun Definition of intellectual content: Junqi Sun, Feifei Shan Clinical studies: Yijie Chen, Jichun Guo, Feifei Shan Data acquisition: Yijie Chen, Jichun Guo Data analysis: Yijie Chen, Jichun Guo Statistical analysis: Feifei Shan Manuscript preparation: Yijie Chen Manuscript editing: Zhihua Meng, Zhensong Chen Manuscript review: Gehua Tong, Junqi Sun.

Funding

This work was supported by the Science and Technology Program of Shaoguan City (No. 210922204531943, No. 230330098033759), Medical Science and Technology Research Fund Project of Guangdong Province (No. B2023468), and Health Research Project of Shaoguan City (No. Y22103, No. Y2023080).

Declarations

Competing interests

The authors declare no competing interests.

Ethics approval and consent to participate

This study was performed according to the Declaration of Helsinki (<https://www.wma.net/what-we-do/medical-ethics/declaration-of-helsinki/>), and approved by the Ethics Commission of Yuebei People's Hospital. Informed consent was obtained from all the participants.

Additional information

Correspondence and requests for materials should be addressed to J.S.

Reprints and permissions information is available at www.nature.com/reprints.

Publisher's note Springer Nature remains neutral with regard to jurisdictional claims in published maps and institutional affiliations.

Open Access This article is licensed under a Creative Commons Attribution-NonCommercial-NoDerivatives 4.0 International License, which permits any non-commercial use, sharing, distribution and reproduction in any medium or format, as long as you give appropriate credit to the original author(s) and the source, provide a link to the Creative Commons licence, and indicate if you modified the licensed material. You do not have permission under this licence to share adapted material derived from this article or parts of it. The images or other third party material in this article are included in the article's Creative Commons licence, unless indicated otherwise in a credit line to the material. If material is not included in the article's Creative Commons licence and your intended use is not permitted by statutory regulation or exceeds the permitted use, you will need to obtain permission directly from the copyright holder. To view a copy of this licence, visit <http://creativecommons.org/licenses/by-nc-nd/4.0/>.

© The Author(s) 2025